
Proceedings Paper:
Ozdemir, B., Khalid, M.A., Valdastri, P. et al. (2026) A Hybrid Tendon-Pneumatic Continuum Robot with Pressure-Driven Length Modulation and Tool-Channel Locking. In: 2026 IEEE 9th International Conference on Soft Robotics (RoboSoft). 2026 IEEE 9th International Conference on Soft Robotics (RoboSoft), 07-12 Apr 2026, Kanazawa, Japan. IEEE, pp. 950-955. ISBN: 979-8-3315-8216-6. ISSN: 2769-4526. EISSN: 2769-4534.

https://doi.org/10.1109/robosoft67810.2026.11522845

A Hybrid Tendon-Pneumatic Continuum Robot with Pressure-Driven Length Modulation and Tool-Channel Locking

Burak Ozdemir, Muhammad A. Khalid, Pietro Valdastri and James H. Chandler

***Abstract*— Continuum robots capable of modulating both their geometry and stiffness are well-suited to the demands of minimally invasive interventions within confined anatomical environments. Existing designs typically achieve either bending through tendon actuation or axial extension via pneumatic chambers, but rarely integrate both functions in a compact architecture. This paper presents a hybrid tendon-pneumatic continuum robot that integrates pressure-driven length modulation and tendon-based steering within a soft thermoplastic elastomer (TPE) body. The tubular robot has a diameter of 14 mm and houses a 4 mm central tool channel. Pressurization enables continuous extension and contraction and reversible tool-channel locking, while three peripheral tendons provide precise directional control. Experimental evaluation demonstrates a pressure-dependent deployment rate up to 70 mm, and a defined 3D workspace. Model validation shows $<$2% relative error between predicted and measured shapes in different backbone configurations. Phantom demonstrations confirm the robot's suitability for confined endoluminal environments, while multi-robot configurations demonstrate the possibility for collaborative, adaptable grasping. The compact geometry, integrated hybrid actuation, and pressure-responsive locking capability represent a promising step toward multifunctional continuum manipulators for medical and industrial applications.**

I. INTRODUCTION

Continuum robots (CRs) have emerged as a versatile class of manipulators capable of performing dexterous tasks in highly constrained environments where conventional rigid-link robots are limited [1], [2]. Their continuously deformable backbones enable smooth bending, intrinsic compliance, and safe interaction with surrounding anatomy, making them well-suited for medical [3], industrial [4], and inspection applications [5] that require flexibility and adaptability. Despite these advantages, the absence of discrete joints makes accurate modeling and control challenging, particularly when balancing compliance and stability.

CRs can be actuated using various methods such as tendons [6], pneumatics [7], hydraulics [8], or magnetic fields [9], with each providing specific benefits and trade-offs. Tendon-driven actuation enables compact proximal control and high precision while maintaining relatively fast response, but suffers from frictional losses, backlash, and tensioning complexity, which can introduce hysteresis and nonlinear behavior [2]. Conversely, pneumatic actuation produces distributed deformation with smooth, compliant motion suitable for safe interaction, but typically presents nonlinear pressure–deformation dynamics which limit repeatability [10].

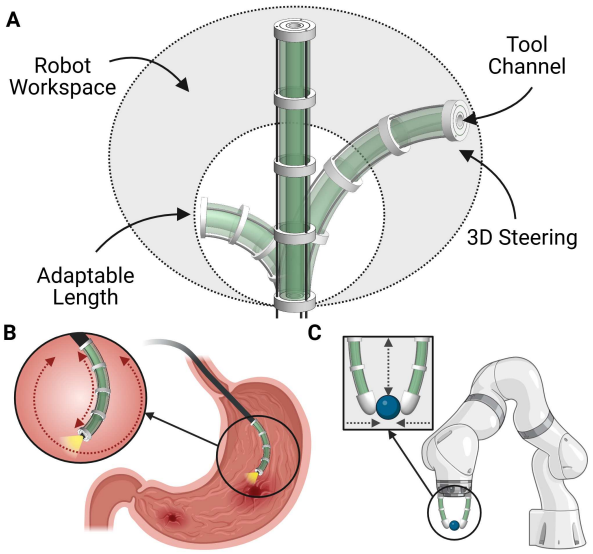

Fig. 1. (A) The hybrid tendon-pneumatic CR with adaptable length and 3-D steering. (B) Gastroscope-style deployment for enhanced steering and workspace in diagnostic or therapeutic procedures. (C) Telescopic CR-based soft gripper for versatile object handling. Created in BioRender. Khalid, M. A. (2026). https://BioRender.com/6p6jg5z

To combine the strengths of both approaches, researchers have proposed hybrid CRs that integrate multiple actuation principles [11]. Among these, hybrid parallel architectures, in which pneumatic and tendon actuation coexist within the same structure, represent a promising direction [10], [12]–[15]. In such systems, pneumatic actuation governs global shape or stiffness modulation, while tendons provide antagonistic forces and precision steering [13]. This parallel hybrid strategy enhances versatility, enabling coordinated control of compliance, extension, and bending. However, many existing designs rely on multi-chamber pneumatic bodies or complex fabrication schemes, limiting miniaturization and restricting integration of a working channel for tool passage [15].

In this work, we introduce a compact hybrid tendon-pneumatic CR utilizing a single-cavity, pressure-driven architecture. The structure comprises a thin thermoplastic elastomer (TPE) inner-outer tube pair connected by 3D-printed disks, forming a 4 mm tool channel within a 14 mm body.

This work was supported in part by the Engineering and Physical Sciences Research Council (EPSRC) under grants EP/Y037235/1 and EP/V009818/1; the European Research Council (ERC) through the European Union's Horizon 2020 Research and Innovation Programme under grant 818045;and the National Institute for Health and Care Research (NIHR) Leeds Biomedical Research Centre (BRC) under grant NIHR203331. B. Ozdemir was supported by a scholarship from the Turkish Ministry of National Education, Republic of Turkiye. J. Chandler was supported by the Leverhulme Trust and the Royal Academy of Engineering under a RAEng/Leverhulme Trust Research Fellowship under grant LTRF-2425-21-154.

Authors are with the School of Electronic and Electrical Engineering, University of Leeds, U.K. Contact: j.h.chandler@leeds.ac.uk

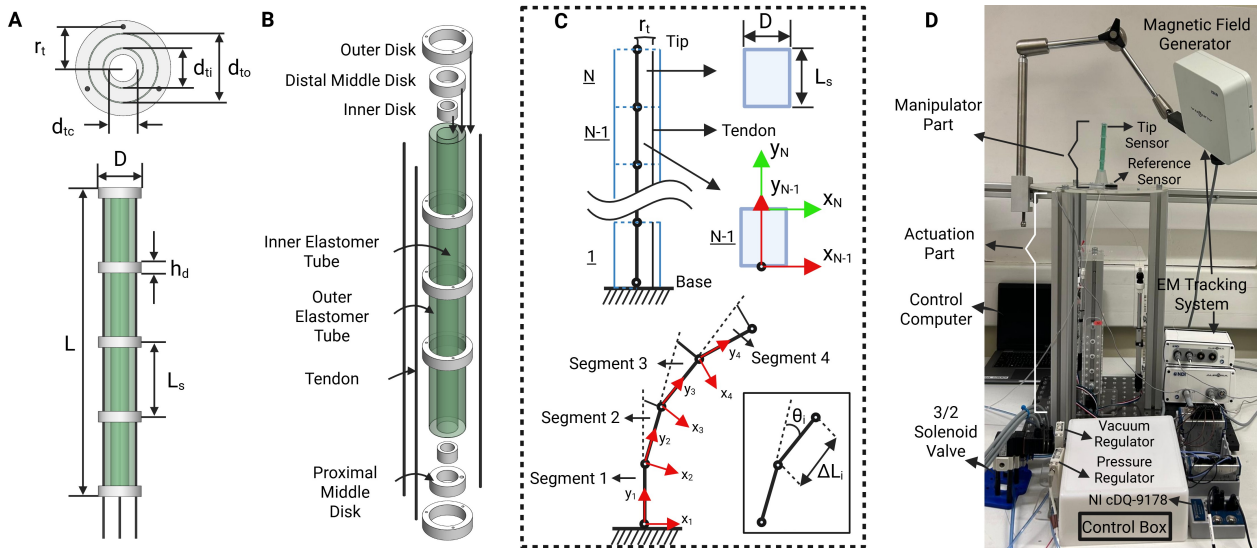

Fig. 2. The hybrid tendon-pneumatic CR, showing: (A) Design parameters, (B) Robot components, (C) Modeling approach, and (D) Experimental setup.

Positive or vacuum pressure applied through a single inlet drives axial extension or contraction, while three distributed tendons achieve directional tip steering. The concept of the proposed hybrid CR is illustrated in Fig. 1(A). A unique feature of the proposed design is its pressure-responsive tool-channel locking mechanism, which uses internal pressure to reversibly fix or release instruments inserted through the lumen. This function allows the same pneumatic system that drives length change to also provide in-situ tool stabilization, introducing enhanced multifunctionality in hybrid continuum actuation. Compared with previously reported hybrid designs [10], [15], the robot achieves mechanical simplicity, functional integration, and structural compactness, showing potential for further miniaturization without design limitations. The controllable length, precise steering, and tool-locking capability of the hybrid tendon-pneumatic manipulator offer new opportunities for both medical applications, such as upper gastrointestinal interventions (Fig. 1(B)), and industrial tasks, including adaptive grasping and compliant manipulation in confined environments (Fig. 1(C)).

II. MATERIALS AND METHODS

A. Design Approach

The proposed tendon-pneumatic hybrid CR utilizes a thin-film TPE formed into a tube with an annulus cross-section as its main body. Two TPE tubes are nested together and sealed at both ends using rigid disks to form a closed chamber for pressure/vacuum actuation and a central tool channel. Under vacuum, the chamber flattens, allowing the body to be collapsed. However, under positive pressure, the chamber forms a tubular shape with pressure dependent stiffness while the tool channel cavity narrows. Three axisymmetric tendons are positioned around the larger tube and aligned using multiple rigid disks along the robot's length. The tendons can slide freely through the disks but are fixed at the distal end. The robot contracts by pulling all tendons simultaneously and can steer in three-dimensional space by pulling one or two tendons at a time. The design parameters are described in Table I, and shown in Fig. 2(A).

The design elements (Fig. 2(B)) and material selection enable specific features. The TPE material itself has negligible stiffness, and the robot relies on the three tendons working in parallel with the pressurized tubular body to support its structure and bending. The proposed design can rapidly extend to full length at relatively low operating pressures of $\leq$20 kPa. The prototype design offers a small diameter of 14 mm with a 4 mm tool channel, and features a contraction ratio of 70% of its original length. The applied pressure and tool integration impact the bending stiffness of the robot; low pressure with no tool creates low bending stiffness, whereas increased pressure and/or integration of flexible tools provides stiffer configurations.

B. Fabrication

The main body of the robot consists of a pneumatic chamber having an outer elastomer tube of 10 mm and an inner elastomer tube of 6 mm. These tubes were fabricated from 38 µm-thick TPE film (Stretchlon 200, Airtech Advanced Materials, UK) by heat-pressing two layers together, followed by cutting a rectangular shape using an optical laser cutter (Creality Falcon 2 Pro 22 W, Creality, China). This process resulted in a sealed rectangular geometry, in which the width of the rectangle represents half of the tube's circumference [16]. This method enables repeatable tube geometry and consistent seam quality across samples. The shorter sealed edges were cut open manually to form the tubes, allowing them to be joined later and to create the air/tool inlet and outlet. Rigid disks were fabricated using a stereolithography (SLA) 3D printer (Clear V5 resin, Form 4, Formlabs, USA). During assembly, cyanoacrylate glue was used to bond the tubes to the disks and secure the disks together. First, an inner disk was attached to one end of the inner elastomer tube, followed by alignment of the middle

TABLE I
DESIGN PARAMETERS OF THE CONTINUUM ROBOT

Symbol	Description	Value
L	Total length of the robot	100 mm
D	Outer diameter of the robot	14 mm
h_d	Height of the disk	3.5 mm
L_s	Length of each segment	25 mm
r_t	Radius of the robot up to each tendon	6.1 mm
d_{tc}	Diameter of the tool channel	4 mm
d_{to}	Diameter of the outer elastomer tube	10 mm
d_{ti}	Diameter of the inner elastomer tube	6 mm

disk and attachment of the outer elastomer tube and outer disk to complete one end of the robot. From the opposite end, the remaining four outer disks and one middle disk were slid onto the outer and inner tubes, respectively, and the three end disks were fixed in the same order as before. Three 0.2 mm diameter NiTi tendons (McMaster-Carr, USA) were passed through the alignment holes in the outer disks and secured at the distal end. The intermediate outer disks were equally spaced along the outer tube, forming four segments. Finally, the proximal middle disk was connected to a 1 mm diameter silicone tube for air supply. Fig. 2(B) shows the exploded view of the assembly.

To create the robotic gripper, a similar fabrication process was followed. Each finger of the gripper consists of a single elastomer tube of 8 mm diameter (i.e. no central tool channel), 50 mm length, and a 12 mm diameter outer disk. The finger tips were made of silicone (DragonSkin 10 Medium, Smooth-On, USA), and have a diameter of 15 mm and a length of 18 mm. Three fingers were mounted on a 3D-printed fixture and arranged to bend inward during actuation. One tendon from each finger was linked together to ensure simultaneous, uniform inward bending, while the remaining two tendons from each finger were paired separately.

C. Modeling Approach

In this study, the hybrid CR is modeled through a force-based rigid-link discretization [17], [18], where the continuous body is divided into N links of segment length $L_s = 25\,\text{mm}$. The total length of the robot is $L_{\text{nom}} = 100\,\text{mm}$ (i.e., $N = 4$). Each link represents one bending section of the robot, and its orientation change is described by the angle θ_i between consecutive segments, as shown in Fig. 2(C).

The tendon force applied at the actuator is denoted by F_{a}. Due to friction along the tendon path, the transmitted force to the ith segment is reduced as

$$F_{\text{eff},i} = F_{\text{a}} - (i-1)\,\Delta F, \tag{1}$$

where $\Delta F = F_{\text{f,total}}/N$ represents the average frictional loss per segment. For a constant tendon offset r_t from the neutral axis, the bending moment at segment i is

$$M_i = r_t\, F_{\text{eff},i}. \tag{2}$$

Assuming linear elastic bending, the equivalent discrete curvature of each segment is defined as

$$\kappa_i = \frac{M_i}{E_{\text{bend}}\, I}, \qquad \Delta\psi_i = \kappa_i\, L_s, \tag{3}$$

where $E_{\text{bend}}I$ represents the effective bending rigidity. Here, ψ_i represents the local bending rotation of segment i, and $\Delta\psi_i$ is its incremental rotation resulting from the applied tendon moment. In the numerical implementation, the model uses the equivalent bending compliance term $k_{\text{bend}} = L_s/(E_{\text{bend}}I)$.

Axial deformation is considered through the axial stiffness $K_{\text{axial}} = E_{\text{axial}}A$, where E_{axial} is the Young's modulus in compression and A the cross-sectional area. Let $\mathbf{f}_i = F_{\text{eff},i}\,\mathbf{n}_i$ be the local tendon force (direction $\mathbf{n}_i$) and $\mathbf{z}_i$ the local tangent. The incremental axial shortening of segment i is

$$\Delta L_{c,i} = \frac{\mathbf{z}_i^{\top}\mathbf{f}_i}{K_{\text{axial}}}\, L_s, \qquad L_{\text{eff},i} = L_s - \Delta L_{c,i}. \tag{4}$$

Starting from the base pose $(\mathbf{p}_1, R_1)$, the backbone shape is computed recursively for each segment:

$$\mathbf{p}_{i+1} = \mathbf{p}_i + R_i\,\mathbf{e}_y\, L_{\text{eff},i}, \tag{5}$$

$$R_{i+1} = R_i\,\exp\big([\mathbf{u}_i]_{\times}\,\Delta\psi_i\big), \tag{6}$$

where $\mathbf{e}_y = [0\ 1\ 0]^{\top}$ is the nominal backbone direction, and $\mathbf{u}_i$ is the local bending axis. The inter-segment angle θ_i is obtained by accumulating the local rotations $\Delta\psi_i$.

This formulation combines the advantages of force-based modeling and rigid-link discretization, capturing both the distributed tendon loading and the resulting geometric deformation [18]. The parameters $\{k_{\text{bend}}, K_{\text{axial}}, \Delta F\}$ were identified through experimental fitting to minimize the shape deviation between simulated and measured configurations. This segment-wise mapping also allows the robot to be modeled at different deployed lengths and to consider the influence of a deployable tool by modulating independent segment length and stiffness parameters. For example, when the backbone is deployed up to segment i, proximal segments are modeled with an increased effective modulus $E^{(i)}_{\text{bend}}I$, reducing the corresponding rotation $\Delta\psi_i$ in Eq. (3) while leaving the distal segments unchanged.

D. Experimental Setup

To evaluate the hybrid CR, an experimental setup was developed as shown in Fig. 2(D). Each tendon was independently actuated using a miniature linear actuator (L12-100-50-12-I, Actuonix) with 100 mm stroke and integrated feedback, driven and monitored via a data acquisition card (cDAQ, National Instruments). A 3D electromagnetic (EM) tracking system (AURORA, NDI) was used to characterize the workspace, with sensors at the base and distal tip of the robot. To record full-shape in-plane bending, a camera with sub-millimeter resolution (Basler aCA2040-120um, 2048 $\times$ 1536 pixels, and calibrated pixel-to-length conversion (<0.1 mm)) was used. Pneumatic actuation was controlled using a pressure (SMC-ITV0010-3BL) and vacuum regulator (SMC-IRV20-C08) connected to a 3/2 solenoid valve, supplying positive or vacuum pressure to the robot chamber. The valves were commanded via NI-cDAQ and a custom interface (LabVIEW, National Instruments, USA).

Details of the experimental procedures (workspace characterization, elongation, dynamic response, and model validation) are provided in Section III.

III. RESULTS

A. Workspace Characterization

To evaluate the reachable space of the proposed hybrid CR, its tip position was tracked over 15,000 randomized tendon displacement input combinations, with one or two tendons actuated simultaneously to values between 0-16 mm. An EM sensor was inserted through the central lumen and fixed at the distal tip to allow 3D tracking of the end position, and the robot's body was maintained at a constant internal pressure of 16 kPa to ensure full elongation throughout.

The resulting workspace reachable by the robot's tip under full extension is presented in Fig. 3. In the top view (X–Z), the reachable boundary forms an approximately 90 mm radius, indicating an approximately circular and symmetrical coverage. In the side view (X–Y), the vertical workspace spans approximately 120 mm, reflecting the effective contribution of the pressure-driven elongation mechanism. The tip is also able to access positions below the base of the robot, as seen under high-angle bending (see Supplementary Video). These results confirm that the combined tendon-pneumatic actuation enables a broad and well-distributed 3D workspace.

B. Elongation and Deployment Analysis

To characterize the axial elongation capability of the proposed robot, the body was incrementally actuated through pneumatic pressurization to reach five distinct configurations, as illustrated in Fig. 4. Each configuration is denoted by L_i $(i = 0, 1, 2, 3, 4)$, where L_0 represents the unactuated initial length of 30 mm.

The segmental elongation within each configuration is represented by L_{e_i} for $i = 1, 2, 3, 4$, corresponding to 25 mm, 50 mm, 75 mm, and 100 mm, respectively. The overall elongation change with respect to the unactuated state is defined as:

$$\Delta L_i = L_i - L_0, \quad (i = 1, 2, 3, 4) \tag{7}$$

The relative extension ratio E_i expresses the percentage elongation of each configuration compared to the initial length, computed as:

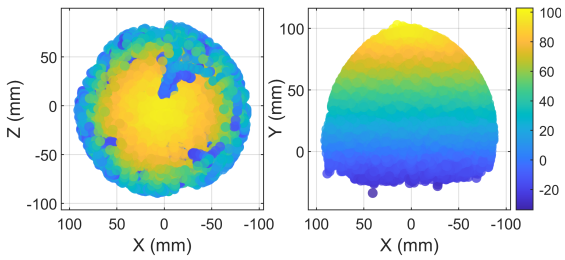

Fig. 3. Workspace characterization results of the hybrid tendon-pneumatic continuum robot: (A) Top view (X-Z) and (B) side view (X–Y) representations of 15,000 randomized tendon actuation combinations, with color indicating the Y-axis displacement of the robot tip.

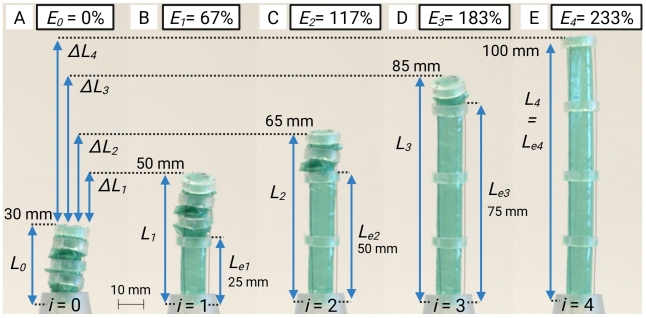

Fig. 4. Stepwise elongation response of the hybrid tendon-pneumatic continuum robot under pneumatic pressure. Configurations (A–E) correspond to elongation states E_0–E_4, illustrating the extension from unactuated length L_0 to maximum length L_4, along with the incremental elongation ΔL_i and segment lengths L_{e_i}.

$$E_i = \frac{L_i - L_0}{L_0} \times 100\% \tag{8}$$

As evident from Fig. 4, the robot can increase its initial length by 233% while maintaining uniform deformation across all sections. These results demonstrate the effective stepwise elongation response achieved through the integrated pneumatic actuation, which enables smooth and repeatable elongation under moderate input pressures (see Supplementary Video).

C. Dynamic Response to Pneumatic Pressure

To evaluate the robot's dynamic stepwise elongation behavior, step-input pressure tests were performed in the range of 4 kPa to 20 kPa, with increments of 4 kPa while the robot's vertical tip position was tracked using a camera. The corresponding elongation ΔL was calculated as a function of time, with each experiment repeated three times. The robot's initial length was collapsed to 30 mm prior to each test and the maximum achievable length under full pressurization for the specific design was ∼100 mm, corresponding to a maximum expected elongation of $\Delta L_{\max} \approx 70$ mm.

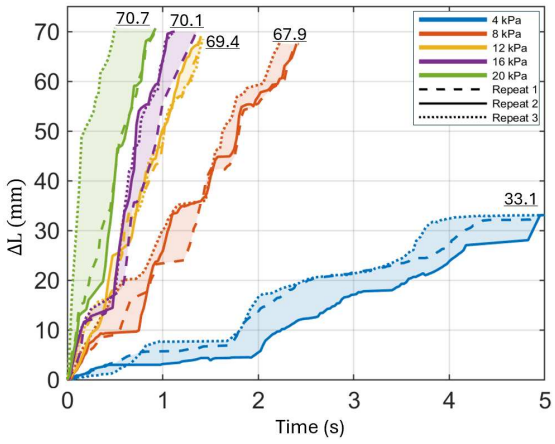

Fig. 5. Dynamic elongation response of the hybrid tendon-pneumatic CR under different pressure inputs. Step pressures ranging from 4 kPa to 20 kPa (in 4 kPa increments) were applied in three repeated trials for each condition, maximum elongation values for each pressure reported in mm.

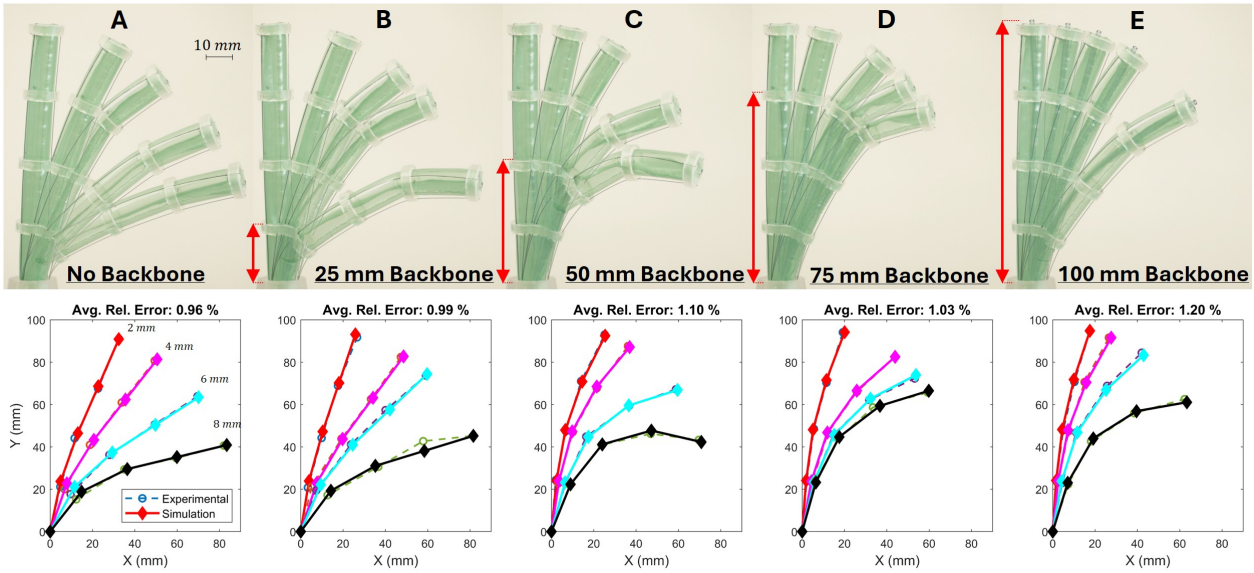

Fig. 6. Model validation of the hybrid tendon-pneumatic continuum robot under different backbone deployment conditions. Configurations (A–E) correspond to backbone insertion lengths of 0, 25, 50, 75, and 100 mm, respectively. For each configuration, a single tendon was actuated with displacements of 2, 4, 6, and 8 mm, and the resulting bending shapes were compared between experimental measurements and model simulation outputs.

As shown in Fig. 5, increased input pressure yields greater ultimate elongation and reduces actuation time to reach maximum elongation. At 20 kPa, the robot achieved $\Delta L = 70.7$ mm in less than one second, while at 4 kPa, the elongation reached a maximum of only $\Delta L = 33.1$ mm after approximately five seconds. The results indicate that higher pressures not only enhance elongation speed but also slightly increase the final displacement due to the elastic deformation of the TPE material, producing a minor overshoot of 0.1–0.7 mm beyond the nominal 70 mm limit.

These findings confirm the pressure-dependent dynamic elongation response of the hybrid tendon-pneumatic structure, where the pneumatic chamber governs elongation rate and amplitude, while the elastic body properties introduce a compliant yet stable saturation behavior under steady-state conditions.

D. Variable Backbone Deployment & Model Validation

Bending behavior and associated suitability of the proposed model were evaluated under different tool deployment conditions. A flexible silicone tube (2 mm outer diameter) was used as the deployable tool, which acts as a flexible backbone to locally increase the stiffness when locked to the robot's body. As shown in Fig. 6, for each test the tool was inserted from the base to one of five configurations (0 mm (no tool), 25 mm, 50 mm, 75 mm, and 100 mm (full deployment)) and locked with 16 kPa body inflation pressure. For each configuration, a single tendon was actuated with displacements of 2 mm, 4 mm, 6 mm, and 8 mm, while the corresponding in-plane bending shape recorded. Tool insertion progressively reduces the effective low-stiffness free bending length of the continuum body, resulting in increased resistance to bending for identical tendon inputs.

The tool/backbone insertion lengths were selected corresponding to L_{e_i} $(i = 0, 1, 2, 3, 4)$ to align with the external disks under full elongation. As shown in Fig. 6, for greater insertion length the overall magnitude of bending decreases and becomes more concentrated toward the distal low stiffness section(s). This trend was consistently reproduced by the simulation results, confirming that the model captured the geometry-dependent stiffness variation using stiffness parameters identified from experimental bending data. The quantitative comparison showed close agreement across all deployment levels, with average relative errors of 0.96%, 0.99%, 1.10%, 1.03%, and 1.20% for configurations spanning from no-backbone to full-backbone, respectively. These sub-2% deviations demonstrate the suitability of the proposed model in capturing the deformation trends observed under different backbone conditions.

E. Endoscopic Robot and Gripper Testing

The proposed hybrid CR was evaluated under manual manipulation inside a scaled-up 3D-printed cross-sectional model of a human stomach Fig. 7A. The robot was first inserted into the stomach phantom in its collapsed state. Once inside, it was pressurized to deploy into the workspace and actuated via its tendons without further proximal push. Tendons' actuation was used to successfully steer and oriented the robot's tip towards the target lesions. Subsequent removal of the pressure and combined tendon actuation allowed the robot to be retracted for removal, demonstrating the potential utility of the hybrid CR for enhanced workspace access in endoluminal applications.

To demonstrate the versatility of the proposed design approach, a three-fingered deployable soft gripper implementation (described in Section II-B) was evaluated by grasping and holding 3D-printed objects of various shapes, as

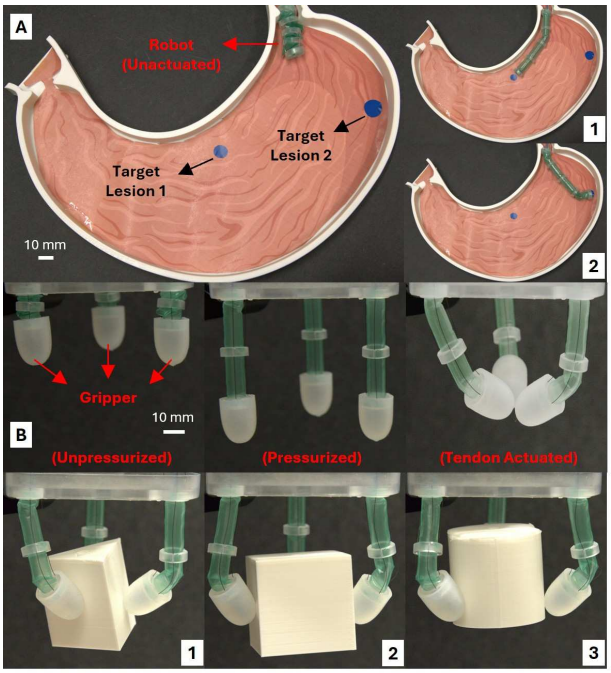

Fig. 7. Demonstration of two application domains. (A) Gastroscopy in a stomach phantom, where the robot is inserted into the lumen and steered toward two target lesions: (1) Target 1; (2) Target 2. (B) Industrial manipulation, where the pneumatic gripper grasps objects in unpressurized and actuated states: (1) cube; (2) triangular prism; (3) cylinder.

shown in Fig. 7(B). Parallel finger deployment and inflation were followed by manual operation of three paired tendons (one per finger) to induce inward bending or all tendons together for simultaneous finger contraction (see Supplementary Video). The gripper effectively grasped and lifted objects of different shapes (triangular prism, cube, and cylinder) due to its flexible fingers, which adapt to object geometry, and a gripping force dependent on the applied pressure and tendon loading. These results show the gripper's utility in situations where advancing a static gripper assembly is not feasible.

IV. CONCLUSION

The results demonstrate that the proposed hybrid tendon-pneumatic CR can achieve controlled elongation, bending, and shape modulation within a compact structure. Integration of pneumatic and tendon actuation enables both axial extension and directional steering, while the pressure-responsive tool-channel locking adds functional versatility. Dynamic characterization showed that higher input pressures produced faster elongation responses, allowing the robot to reach its maximum length in a shorter time. From the unactuated state to the fully pressurized condition, the robot achieved a 233% increase in length and demonstrated high bending angles ($>180°$), confirming its wide and controllable deformation range. The modeling framework matched the experimental deformation behavior across backbone configurations, although further calibration with force data would be needed to develop a fully predictive model. Moreover, the phantom and gripper demonstrations highlight the potential of this design for both medical (gastroscopic) and industrial manipulation tasks. Future work will focus on closed-loop control implementation and miniaturization to enable in vivo deployment and higher precision manipulation.

REFERENCES

[1] J. Burgner-Kahrs, D. C. Rucker, and H. Choset, "Continuum robots for medical applications: A survey," *IEEE Transactions on Robotics*, vol. 31, no. 6, pp. 1261–1280, 2015.

[2] T. da Veiga, J. H. Chandler, P. Lloyd, G. Pittiglio, N. J. Wilkinson, A. K. Hoshiar, R. A. Harris, and P. Valdastri, "Challenges of continuum robots in clinical context: a review," *Progress in Biomedical Engineering*, vol. 2, no. 3, p. 032003, 2020.

[3] L. Z. Yañez, J. Rogatinsky, D. Recco, S.-Y. Lee, G. Matthews, A. P. Sabelhaus, D. Hoganson, and T. Ranzani, "Soft robotic delivery of coiled anchors for cardiac interventions," *IEEE Robotics and Automation Letters*, pp. 1–8, 2025.

[4] M. P. H. Niño, M. Boutayeb, and D. Martinez, "A hybrid tendon-driven continuum robot that avoids torsion under external load," *Frontiers in Robotics and AI*, vol. 12, p. 1576209, 2025.

[5] M. Wang, X. Dong, W. Ba, A. Mohammad, D. Axinte, and A. Norton, "Design, modelling and validation of a novel extra slender continuum robot for in-situ inspection and repair in aeroengine," *Robotics and Computer-Integrated Manufacturing*, vol. 67, p. 102054, 2021.

[6] T. Kato, I. Okumura, S.-E. Song, A. J. Golby, and N. Hata, "Tendon-driven continuum robot for endoscopic surgery: Preclinical development and validation of a tension propagation model," *IEEE/ASME Transactions on Mechatronics*, vol. 20, no. 5, pp. 2252–2263, 2014.

[7] R. Kang, D. T. Branson, T. Zheng, E. Guglielmino, and D. G. Caldwell, "Design, modeling and control of a pneumatically actuated manipulator inspired by biological continuum structures," *Bioinspiration & biomimetics*, vol. 8, no. 3, p. 036008, 2013.

[8] J. Liu, L. Yin, J. H. Chandler, X. Chen, P. Valdastri, and S. Zuo, "A dual-bending endoscope with shape-lockable hydraulic actuation and water-jet propulsion for gastrointestinal tract screening," *The International Journal of Medical Robotics and Computer Assisted Surgery*, vol. 17, no. 1, pp. 1–13, 2021.

[9] P. Lloyd, T. L. Thomas, V. K. Venkiteswaran, G. Pittiglio, J. H. Chandler, P. Valdastri, and S. Misra, "A magnetically-actuated coiling soft robot with variable stiffness," *IEEE Robotics and Automation Letters*, vol. 8, no. 6, pp. 3262–3269, 2023.

[10] J.-Y. Lee, E.-Y. Go, W.-Y. Choi, W.-B. Kim, and K.-J. Cho, "Development of soft continuum manipulator with pneumatic and tendon driven actuations," in *2016 13th International Conference on Ubiquitous Robots and Ambient Intelligence (URAI)*. IEEE, 2016, pp. 377–379.

[11] B. Ozdemir, M. A. Khalid, M. Chauhan, P. Valdastri, and J. H. Chandler, "Hybrid continuum robot designs and architectures for healthcare applications," *Advanced Robotics Research*, p. e202500177, 2026.

[12] J. Hu, J. Zhang, Y. Zheng, B. Wang, J. Wu, X. Wang, and Y. Yang, "Hybrid-driven continuum robot with decoupled motion patterns for dexterous manipulation," *IEEE Robotics and Automation Letters*, 2024.

[13] X. Luo, D. Song, Z. Zhang, S. Wang, and C. Shi, "A novel distal hybrid pneumatic/cable-driven continuum joint with variable stiffness capacity for flexible gastrointestinal endoscopy," *Advanced Intelligent Systems*, p. 2200403, 2023.

[14] M. Roshanfar, J. Dargahi, and A. Hooshiar, "Design optimization of a hybrid-driven soft surgical robot with biomimetic constraints," *Biomimetics*, vol. 9, no. 1, p. 59, 2024.

[15] Z. Zhang, S. Tang, W. Fan, Y. Xun, H. Wang, and G. Chen, "Design and analysis of hybrid-driven origami continuum robots with extensible and stiffness-tunable sections," *Mechanism and Machine Theory*, vol. 169, p. 104607, 2022.

[16] J. Davy, T. P. Dean, N. J. Greenidge, B. Calmé, P. Lloyd, J. H. Chandler, and P. Valdastri, "Magnetic fluid-driven vine robots for minimally invasive tissue biopsy sampling," *Advanced Intelligent Systems*, vol. 7, no. 8, p. 2400827, 2025.

[17] J. Zhang and N. Simaan, "Design of underactuated steerable electrode arrays for optimal insertions," *Journal of Mechanisms and Robotics*, vol. 5, no. 1, p. 011008, 2013.

[18] B. Ozdemir, P. Valdastri, and J. H. Chandler, "Towards accurate shape prediction for compact spring backbone tendon-driven continuum robots," in *Annual Conference Towards Autonomous Robotic Systems*. Springer, 2025, pp. 210–222.